Intramolecularly Protein-Crosslinked DNA Gels: New Biohybrid Nanomaterials with Controllable Size and Catalytic Activity

Li Zhou, Mathieu Morel, Sergii Rudiuk, and Damien Baigl**

DNA micro- and nanogels—small-sized hydrogels made of a crosslinked DNA backbone—constitute new promising materials, but their functions have mainly been limited to those brought by DNA. Here a new way is described to prepare sub-micrometer-sized DNA gels of controllable crosslinking density that are able to embed novel functions, such as an enzymatic activity. It consists of using proteins, instead of traditional base-pairing assembly or covalent approaches, to form crosslinks inside individual DNA molecules, resulting in structures referred to as intramolecularly protein-crosslinked DNA gels (IPDGs). It is first shown that the addition of streptavidin to biotinylated T4DNA results in the successful formation of thermally stable IPDGs with a controllable crosslinking density, forming structures ranging from elongated to raspberry-shaped and pearl-necklace-like morphologies. Using reversible DNA condensation strategies, this paper shows that the gels can be reversibly actuated at a low crosslinking density, or further stabilized when they are highly crosslinked. Finally, by using streptavidin–protein conjugates, IPDGs with various enzymes are successfully functionalized. It is demonstrated that the enzymes keep their catalytic activity upon their incorporation into the gels, opening perspectives ranging from biotechnologies (e.g., enzyme manipulation) to nanomedicine (e.g., vectorization).

1. Introduction

Besides its biological importance, DNA can be seen as a material that combines unique properties of biocompatibility and programmability.[1–5] For instance, the use of DNA as a backbone for hydrogels has recently led to various fundamental studies[6–8] and applications,[9–11] such as molecular detection,[12] drug or gene delivery,[13,14] cell culture,[15] and water detoxification.[16,17] Such DNA hydrogels can be prepared by several methods, including covalent crosslinking between double-stranded DNA molecules,[18] i-motif formation or hybridization between sticky ends of branched DNA nanostructures,[6,19–21] and physical entangling between long DNA strands.[22] For nanotechnological and biomedical applications, the reduction of the dimensions[23–25] of such biocompatible materials is often a requisite, which has triggered a growing interest for nano- and microsized DNA gels. For instance, DNA nanogels of controllable size were prepared through hybridization between branched DNA nanostructures in the presence of DNA units able to inhibit the extension of the nanogel.[13] Another strategy has relied on the intramolecular hybridization inside long, single-stranded DNA produced by the rolling circle amplification method.[26]

Dr. L. Zhou, Dr. M. Morel, Dr. S. Rudiuk, Prof. D. Baigl
PASTEUR
Department of Chemistry
École normale supérieure
UPMC Univ. Paris 06
CNRS, PSL Research University
75005 Paris, France
E-mail: sergii.rudiuk@ens.fr; damien.baigl@ens.fr
Dr. L. Zhou, Dr. M. Morel, Dr. S. Rudiuk, Prof. D. Baigl
Sorbonne Universités
UPMC Univ. Paris 06
Ecole normale supérieure, CNRS
PASTEUR, 75005 Paris, France

DOI: 10.1002/smll.201700706

 © 2017 Wiley-VCH Verlag GmbH & Co. KGaA, Weinheim

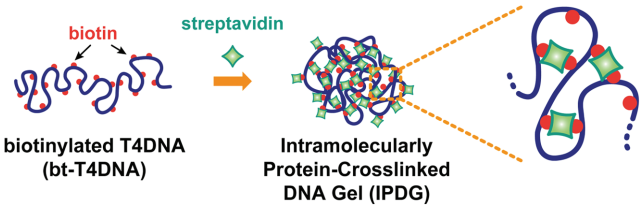

Figure 1. Streptavidin induces the crosslinking of biotinylated DNA (bt-T4DNA) into intramolecularly protein-crosslinked DNA gel (IPDG).

These hybridization-based methods have the advantage to exploit the programmability of DNA base-pairing principles, but lead to temperature-sensitive systems.[6] An alternative has consisted of preparing nanogels through covalent crosslinking between either X-shaped DNA nanostructures[27] or condensed plasmid DNA.[28,29] However, with covalent-based approaches, the crosslinking density is determined by the conditions of the crosslinking reaction, hampering possibility to further modify the gel properties once it has been prepared. Here we describe a new methodology for intramolecular DNA gelation, which uses single molecules of giant, comb-like biotinylated DNA as the starting material. With this method, by exploiting the strong yet noncovalent streptavidin/biotin binding characteristics, adding a controlled amount of streptavidin to biotinylated DNA allowed us to form intramolecularly protein-crosslinked DNA gels (IPDGs) (**Figure 1**) for the first time, and tune the gel characteristics (size, crosslinking density) in a user-defined fashion. Moreover, the functionality of DNA micro- and nanogels reported so far has been mainly limited to the inherent physicochemical characteristics of their main constituent, that is, DNA.[14,16,17] By contrast, other types of nanogels, such as organic nanogels, have been demonstrated as versatile and useful hosts for functional entities, such as proteins.[24,25,30–32] Finding ways to functionalize DNA nanogels, for instance, with proteins, thus appears as a valuable challenge. With our method, this was achieved in a straightforward manner by using streptavidin–protein conjugates, thus exploiting streptavidin as both the DNA crosslinking agent and the vector for the protein guest. Here, we describe the preparation of IPDGs, study their structural properties as a function of streptavidin concentration, explore the possibility to further actuate those using DNA condensing/unfolding strategies, and characterize the enzymatic activity of IPDGs functionalized with various enzymes.

2. Results and Discussion

First, we reacedt giant T4DNA (166 000 base pairs (bp)) with psoralen-PEG$_3$-biotin, a photoreactive reagent able to bind DNA through covalent [2 + 2] cycloaddition with pyrimidine bases upon UV exposure[33] (Figure S1, Supporting Information). This led to the formation of biotinylated T4DNA (bt-T4DNA). The incorporation efficiency was estimated to be 1 biotin per 10.5 base pairs using the HABA assay.[34] Streptavidin (strep) was then added to bt-T4DNA to create intramolecular crosslinks between the biotinylated sites and induce noncovalent folding of the DNA molecules. This resulted in single-DNA gel-like structures, referred to as intramolecularly protein-crosslinked DNA gels (IPDGs, Figure 1). In order to achieve crosslinking exclusively at the intramolecular level, the concentration of T4DNA was kept very low (33.6×10^{-9} M in bp, corresponding to 0.2×10^{-12} M in DNA molecules). At this concentration, the average distance between DNA molecules was around 20 µm. This was about one order of magnitude larger than the average long-axis length of DNA measured under our experimental conditions (**Figure 2**), confirming that DNA chains were in a dilute regime during the crosslinking reaction.

To observe the DNA folding process upon streptavidin addition, we used fluorescence microscopy to characterize the

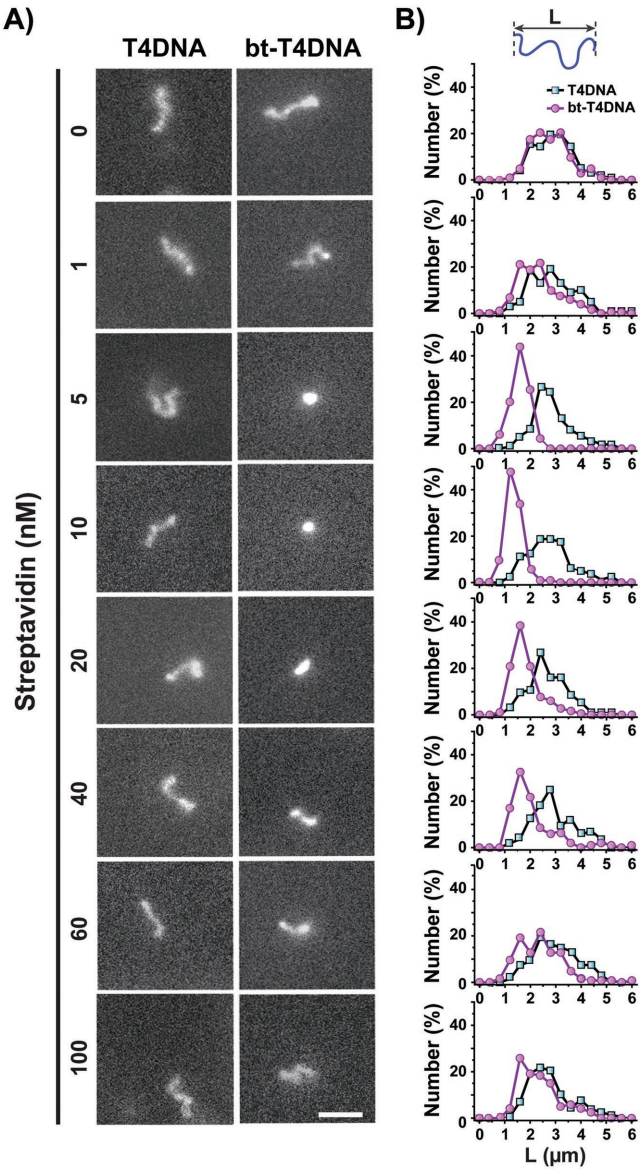

Figure 2. Fluorescence microscopy study of streptavidin-assisted IPDG formation. A) Typical fluorescence microscopy images of non-biotinylated (left) and biotinylated (right) T4DNA in solution as a function of streptavidin concentration. [DNA] = 33.6×10^{-9} M bp; [YOYO] = 10×10^{-9} M; [Tris/HCl] = 10×10^{-3} M (pH = 7.4). Scale bar is 2 µm. B) Long-axis length (L) distribution of over 100 individual T4DNA and bt-T4DNA molecules at different streptavidin concentrations.

© 2017 Wiley-VCH Verlag GmbH & Co. KGaA, Weinheim

behavior (Figure 2A) and to measure the apparent long-axis length (L, Figure 2B) of a large number of DNA molecules in solution, as a function of [strep]. In the absence of strep, both non-biotinylated (T4DNA) and bt-T4DNA behaved as fluctuating elongated coils due to the electrostatic repulsion between negatively charged phosphate groups. Their average long-axis length $\langle L \rangle$ was similar, showing that the biotinylation reaction did not affect the DNA characteristics much. However, T4DNA and bt-T4DNA had a markedly different response to the addition of strep. As expected, strep had no influence on T4DNA molecules, which maintained as fluctuating coils with a similar size regardless of [strep] ($\langle L \rangle = 2.7 \pm 0.6$ µm). By contrast, bt-T4DNA progressively shrunk from elongated coils ($\langle L \rangle = 2.6 \pm 0.7$ µm) to more compact and fast-diffusing globules ($\langle L \rangle = 1.2 \pm 0.3$ µm) with an increase in [strep] from 1×10^{-9} to 10×10^{-9} M. This is in agreement with the formation of IPDG structures that became more compact with an increase in the number of streptavidin-induced intramolecular crosslinks. Strikingly, a further increase in [strep] was accompanied by the opposite trend. bt-T4DNA molecules progressively expanded again, denoting a progressive swelling of the IPDGs, to reach a size of $\langle L \rangle = 2.2 \pm 0.7$ µm at [strep] = 100×10^{-9} M. This expansion was attributed to the saturation of biotin sites by the growing excess of strep, therefore decreasing the crosslinking density inside the IPDGs. Interestingly, the same compaction–expansion behavior as a function of [strep] was observed with bt-T4DNA of other biotinylation rates (Figure S2, Supporting Information). Both the degree of compaction and the concentration of streptavidin to reach optimal compaction decreased with a decrease in the biotinylation rate. All these results show that streptavidin induces multiple crosslinks inside individual biotinylated giant DNAs, leading to DNA gels of controllable size, the highest crosslinking density being obtained at an intermediate streptavidin concentration.

Atomic force microscopy (AFM) characterization was then carried out to provide structural information on the IPDGs obtained with different streptavidin concentrations. For each given [strep], large-scale observations showed a rather homogenous sample distribution in size and morphology (**Figure 3**A; Figures S3 and S4, Supporting Information). Higher-resolution observations (Figure 3B) revealed that, with an increase in [strep], the entities evolved from elongated to raspberry-shaped structures ([strep] ≤ 10×10^{-9} M) before expanding to pearl-necklace-like morphologies ([strep] > 10×10^{-9} M). In the absence of strep, bt-T4DNA appeared as threads with an average height of 0.48 ± 0.07 nm, in agreement with previous observations on DNA adsorbed on mica.[35–37] In the presence of strep, the bright spots observed in both raspberry and pearl-necklace structures had an average height of 1.6 ± 0.6 nm, a value similar to the height of free streptavidin adsorbed on mica (Figure S5, Supporting Information), and were thus attributed to streptavidin crosslinks. We finally characterized the thermal stability of IPDGs in the maximal compaction state (raspberry structures, [strep] = 10×10^{-9} M) by incubating those for 4 h at temperatures ranging from 20 to 65 °C. Regardless of temperature, we did not detect any significant change in the morphology (Figure 3C) nor in the size (Figure S6, Supporting Information) of the IPDGs, demonstrating their stability even at a high temperature. All these results further demonstrate the role of streptavidin as a new crosslinking agent for thermally stable, intramolecular gelation of biotinylated DNA.

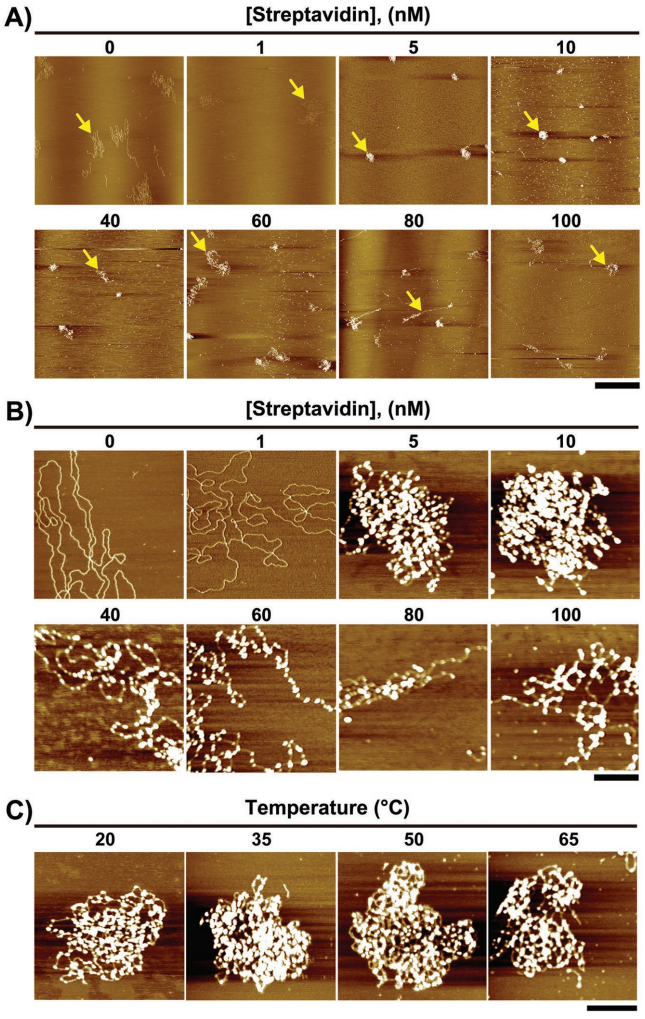

Figure 3. AFM observation and thermal stability of IPDGs. A) Large-scale overview and B) zoomed AFM images of bt-T4DNA incubated with an increasing concentration of streptavidin. Each yellow arrow in (A) indicates the IPDG scanned in (B). C) IPDGs obtained with [strep] = 10×10^{-9} M after 4 h incubation at different temperatures. Scale bars are A) 3 µm and B,C) 300 nm.

According to the biotinylation rate of T4DNA, the fraction of DNA base pairs involved in the formation of the crosslinks was less than 10%. We therefore explored the possibility to further actuate the gels by reversible condensation of the non-crosslinked segments of the DNA backbone. This was done by using spermine (SPM), a naturally occurring DNA compaction agent, and an excess of NaCl as the spermine antagonist.[38–40] We analyzed the effects of sequential addition of SPM (5×10^{-6} M) and NaCl (100×10^{-3} M) to the three typical structures: elongated ([strep] = 1×10^{-9} M), raspberry ([strep] = 10×10^{-9} M), and pearl-necklace ([strep] = 100×10^{-9} M). Fluorescence microscopy observations showed that adding SPM had no effect on the apparent size of the raspberry structures, whereas both elongated and pearl-necklace

 © 2017 Wiley-VCH Verlag GmbH & Co. KGaA, Weinheim

structures became more compact (**Figure 4**A,B). Interestingly, further addition of NaCl induced a recovery of the initial apparent size only in the case of the elongated structures. AFM was then used to characterize the fine structure of the IPDGs under these conditions (Figure 4C). Upon SPM addition, the elongated structures at [strep] = 1×10^{-9} M formed compact, highly looped flower-like structures, reminiscent to the morphologies typically observed during compaction of non-biotinylated DNA.[41–43] Upon addition of NaCl, the structures were elongated again, in agreement with the salt-induced unfolding observed by fluorescence microscopy, which indicated successful decondensation of the DNA backbone by the excess of monovalent salt. The raspberry-like morphologies at [strep] = 10×10^{-9} M became slightly denser upon addition of SPM, showing that DNA segments could be locally condensed by SPM but the large number of streptavidin crosslinks prevented from a large reduction of the IPDG size. The SPM addition to the pearl-necklace structures at [strep] = 100×10^{-9} M also led to tightly compact structures. In agreement with fluorescence microscopy results, the compact structures obtained after SPM addition on raspberry ([strep] = 10×10^{-9} M) and pearl-necklace ([strep] = 100×10^{-9} M) morphologies were not affected much by the addition of NaCl. We suggest that, in the latter case, SPM-induced DNA condensation favored the formation of intramolecular contacts and therefore the creation of additional crosslinks. This shows that SPM can be used as a mean to stabilize DNA gels. All these results demonstrate that, depending on the crosslinking density of the IPDGs, DNA condensation strategies can be used either to reversibly actuate the gels (low [strep]) or to get highly stable compact structures (middle to high [strep]).

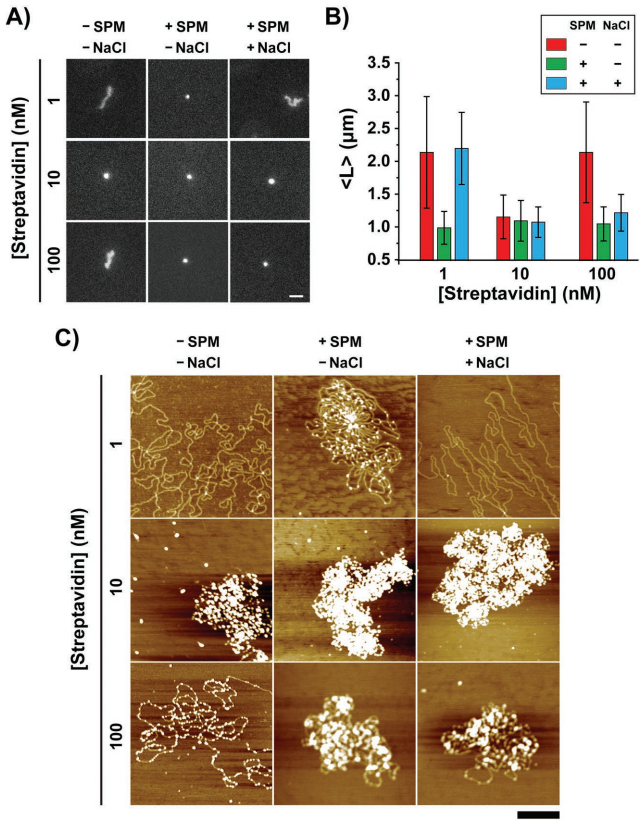

Figure 4. IPDG actuation through reversible DNA condensation. A) Fluorescence microscopy images, B) average long-axis length, and C) representative AFM images for three IPDGs formed at [strep] = 1×10^{-9} M, 10×10^{-9} M, or 100×10^{-9} M, in the absence or in presence of 5×10^{-6} M spermine (SPM) and/or 100×10^{-3} M NaCl. Scale bars are 2 μm (A) and 300 nm (C). Data in (B) are mean ± sd on over 100 individual IPDGs.

Finally, we explored the possibility of functionalizing the gels without any additional step, by directly crosslinking bt-T4DNA with conjugates composed of a streptavidin linked to a desired functional entity such as, for instance, another protein. We studied in particular the possibility of introducing β-galactosidase (βGal), alkaline phosphatase (ALP), or horseradish peroxidase (HRP) enzymes into IPDGs by crosslinking bt-T4DNA with the corresponding streptavidin–enzyme conjugate (strep–βGal, strep–ALP, or strep–HRP, respectively) (**Figure 5**A). Fluorescence microscopy observations showed that the addition of strep–enzyme conjugates led to the same compaction behavior of bt-T4DNA as that with bare streptavidin (Figure S7, Supporting Information), indicating the successful formation of IPDGs. The maximum of crosslinking density was also observed at intermediate strep–enzyme concentrations (Figure 5B), at values slightly higher but close to that with bare streptavidin. To assess the catalytic activity of the resulting functionalized gels, we prepared enzyme-loaded IPDGs using a strep–enzyme concentration leading to highly crosslinked gels, while minimizing the possible excess of unbound enzymes (30×10^{-9} M strep–βGal, 20×10^{-9} M strep–ALP, or 20×10^{-9} M strep–HRP). Enzymatic activity was then measured for each protein after the same incubation time used for the crosslinking reaction (4 °C for 2 h) and normalized to that of the enzyme before the crosslinking reaction (Figure 5C). For both strep–βGal and strep–ALP, these conditions did not affect much the activity of the enzyme, either alone (control 1) or in the presence of individual components such as psoralen-PEG_3-biotin (control 2) or T4DNA (control 3). By contrast, strep–HRP was found to partially loose its activity during the incubation time (control 1), an effect that was slightly diminished in the presence of psoralen-PEG_3-biotin (control 2) or T4DNA (control 3). Notably, when the incubation was performed in the presence of bt-T4DNA (Figure 5C, IDPG), i.e., when intramolecular DNA crosslinking occurred, all strep–enzymes had an activity similar to or higher than that of the unbound strep–enzyme. Knowing that, under these conditions, a significant fraction of strep–enzymes were involved in crosslinking bt-T4DNA, these results show that the three tested enzymes remained functional upon their incorporation into the gels, with a catalytic activity comparable or even higher than that of the free strep–enzymes. The enhancement of the enzymatic activity observed for strep–HRP upon its loading into the IPDG can be either attributed to a protection by the gel microenvironment against protein degradation or explained by an enhancement of the catalytic activity of the bound enzymes due to confinement and/or proximity of DNA. These two effects are already known for enzymes conjugated to DNA in other configurations,[40,44–48] but have never been described for enzymes loaded in DNA microgels.

 © 2017 Wiley-VCH Verlag GmbH & Co. KGaA, Weinheim

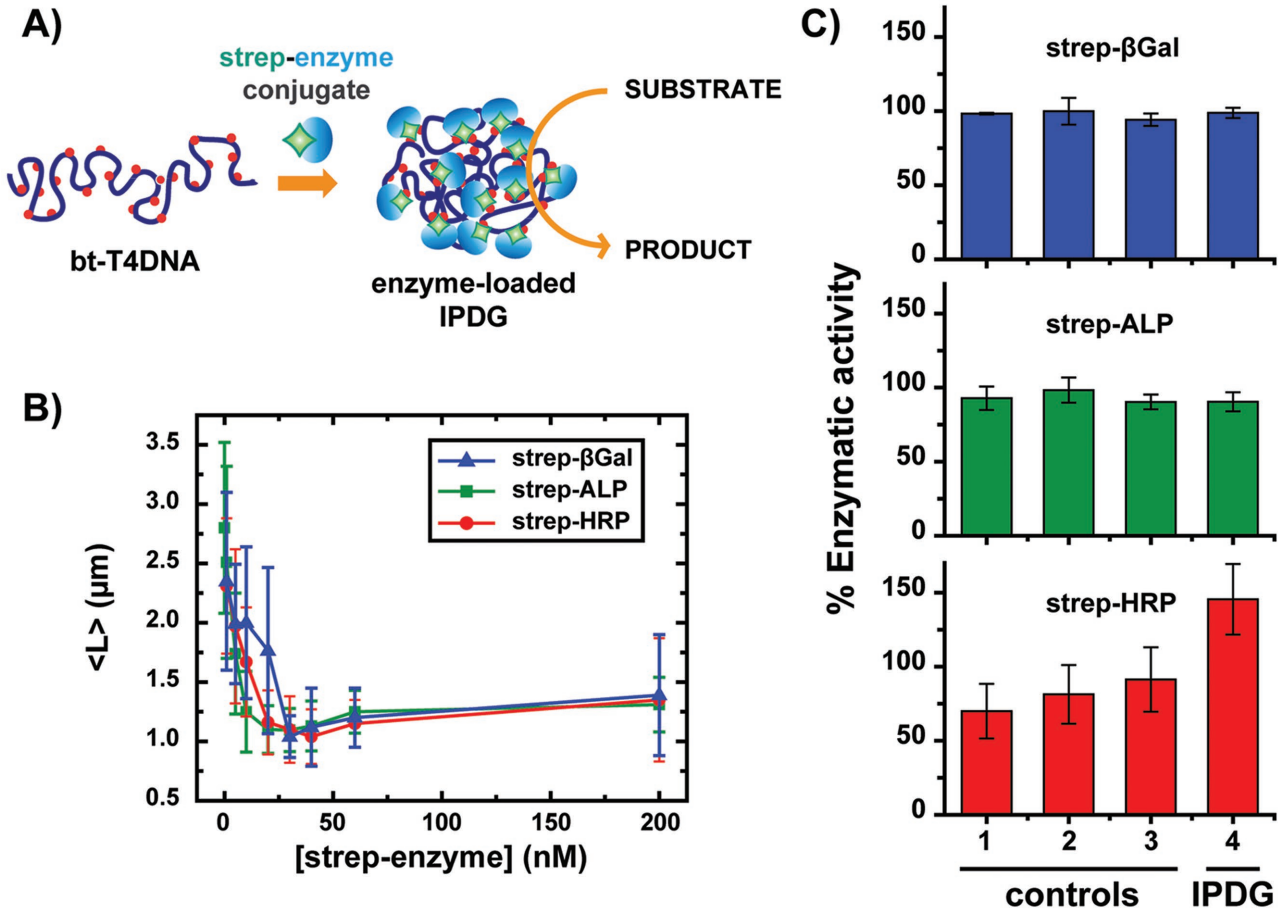

Figure 5. Functionalization of the IPDGs with enzymes. A) Streptavidin–enzyme (strep–enzyme) conjugates are used to crosslink bt-T4DNA, resulting in enzyme-loaded IPDGs. B) Average long-axis length (mean ± sd on over 50 individual objects) of the IPDGs as function of strep–enzyme concentration. C) Enzymatic activities (mean ± sd) of strep–βGal, strep–ALP, and strep–HRP, after the same incubation conditions used for the crosslinking reaction (4 °C for 2 h) for unconjugated enzymes (controls 1–3) and enzymes bound to the IPDG (4). All enzymatic activities were normalized by the activity of the strep–enzyme before the crosslinking reaction. 1: strep–enzyme alone; 2: strep–enzyme + psoralen-PEG_3-biotin; 3: strep–enzyme + T4DNA; 4: strep–enzyme + bt-T4DNA.

All these results show that IPDGs can acquire enzymatic activity upon crosslinking biotinylated DNA with streptavidin–enzyme conjugates.

3. Conclusions

In summary, we have described a new way to create crosslinks inside individual DNA molecules, by exploiting the strong yet noncovalent streptavidin–biotin interaction. We showed that streptavidin allowed us not only to control the crosslinking density of IPDGs, but also to incorporate various protein guests by using commercially available streptavidin–protein conjugates. This method can be readily extended to other proteins or to bring other functions to the DNA gels by using, for instance, streptavidin conjugated to other entities such as nanoparticles or signaling molecules. Another way to functionalize the IPDGs would consist in using biotinylated compounds that could be incorporated in the already formed gels by interacting with the free binding sites of the streptavidin crosslinks. We have also demonstrated the interest of using a reversible DNA condensation strategy to further actuate the IPDGs. This was shown here with the simple spermine/NaCl system but this principle could be extended to other types of DNA compaction processes. For instance, IPDGs could be photocontrolled by using photoreversible DNA compaction systems.[41,49–51] Overall, this work provides insights for the design of novel nano- to microscale multifunctional DNA materials, offering promising perspectives for the development of hybrid DNA/protein-based sensors and reactors.

4. Experimental Section

Materials: Bacteriophage T4 DNA (166 kbp) was purchased from Wako Chemicals. Psoralen-PEG_3-biotin was from G-Bioscience. Streptavidin was obtained from Invitrogen. Streptavidin conjugated to enzymes: β-galactosidase (strep–βGal), alkaline phosphatase (strep–ALP), and horseradish peroxidase (strep–HRP), corresponding substrates (DDAO–galactoside, DDAO–phosphate, and Amplex Red), and YOYO-1 iodide were from Life Technologies. All other chemicals were purchased from Sigma-Aldrich. Deionized MQ water (Millipore, 18 MΩ cm) was used for all experiments.

 © 2017 Wiley-VCH Verlag GmbH & Co. KGaA, Weinheim

Preparation of bt-T4DNA: Psoralen-PEG_3-biotin was dissolved in DMSO to give 20×10^{-3} M stock solution. Reaction mixture (100 µL) was then prepared by mixing T4 DNA (20 µg mL^{-1}, 50 µL) and psoralen-PEG_3-biotin (20×10^{-3} M, 1 µL) in TE buffer (10×10^{-3} M Tris, 1×10^{-3} M EDTA, pH 7.4). The final concentration of T4 DNA was thus 10 µg mL^{-1} (15×10^{-6} M bp) and of psoralen-PEG_3-biotin 0.2×10^{-3} M. The reaction tube was then placed on ice and irradiated with 365-nm UV for 30 min for all data except for Figure S2 (Supporting Information), where shorter UV irradiation times were used to decrease the biotinylation rate. DNA was then purified by size exclusion chromatography using NAP-5 columns (GE Healthcare). The concentration of the resulting biotinylated DNA (bt-T4DNA) was estimated by absorption using BioPhotometer plus spectrophotometer (Eppendorf) to be about 1.4×10^{-6} M bp. After the purification, biotin incorporation was measured using HABA method.[34] According to the decrease of the absorption at 500 nm of HABA upon biotin binding to avidin, the concentration of biotin on bt-T4DNA was about 0.133×10^{-6} M, that is, 1 biotin per 10.5 base pairs for 30 min UV irradiation.

Preparation of the IPDG: 12 µL of bt-T4DNA solution (1.4×10^{-6} M), streptavidin of a desired concentration, Tris/HCl buffer, and MQ water were mixed to give 500 µL solution in 10×10^{-3} M Tris/HCl buffer (pH = 7.4). The concentration of bt-T4DNA in the final mixture was 33.6×10^{-9} M bp. The mixture was incubated either at room temperature for 1 h with bare streptavidin (Figures 1, 2, 3, 4), or at 4 °C for 2 h in the case of streptavidin–enzyme conjugates (Figure 5). For control experiments, the same procedure has been followed with either no DNA, non-biotinylated T4DNA (33.6×10^{-9} M) or psoralen-PEG_3-biotin (3.2×10^{-9} M). For enzymatic activities measurements (Figure 5), IPDGs were prepared with 30×10^{-9} M strep–βGal, 20×10^{-9} M strep–ALP, and 20×10^{-9} M strep–HRP.

Enzymatic Activity Measurements:

β-Galactosidase (βGal): The enzymatic activity assay of strep–βGal was carried out using a fluorogenic DDAO galactoside (DDAOG) substrate, which undergoes hydrolysis of its β-galactoside bond by β-galactosidase, leading to a far-red shift of its fluorescence emission. For the enzymatic activity experiment, 1.67 µL of the sample (IPDG or control solutions) was first diluted to 98.5 µL in 10×10^{-3} M Tris/HCl buffer (pH 7.4) to give 0.5×10^{-9} M final concentration of the enzyme. Then 1.5 µL of DDAOG substrate (5×10^{-3} M) was rapidly added to give the final concentration 75×10^{-6} M, and immediately after mixing, the fluorescence emission intensity at 645 nm (40 nm bandpass) was monitored upon excitation at 590 nm (20 nm bandpass) as a function of time.

Alkaline Phosphatase (ALP): The enzymatic activity assay of strep–ALP was carried out using fluorogenic DDAO-phosphate (DDAOP) substrate, which undergoes hydrolysis of its phosphate bond by ALP, leading to a far-red shift of its fluorescence. For the enzymatic activity experiment, the sample (IPDG or control solutions) was first diluted 6.7 times in 10×10^{-3} M Tris/HCl buffer (pH 8.5) to give 3×10^{-9} M final concentration of the enzyme. Then 0.5 µL of DDAOP substrate (2×10^{-3} M) was rapidly added to give the final concentration 10×10^{-6} M, and immediately after mixing, the fluorescence emission intensity at 645 nm (40 nm bandpass) was monitored upon excitation at 590 nm (20 nm bandpass) as a function of time.

Horseradish Peroxidase (HRP): The enzymatic activity assay of strep–HRP was performed by measuring the initial oxidation rate of Amplex Red with H_2O_2. For the enzymatic activity experiment, the sample (IPDG or control solutions) was first diluted 200 times in 10×10^{-3} M Tris/HCl buffer (pH 7.4) to give 0.1×10^{-9} M final concentration of the enzyme. Amplex Red substrate and H_2O_2 were then added in reaction solutions to give the final concentrations 5×10^{-6} M and 1×10^{-3} M, respectively. The experiment was monitored by measuring the fluorescence change at 590 nm (25 nm bandpass) upon excitation of 530 nm (35 nm bandpass) as function of time.

Enzymatic Activity Assay: All enzymatic reactions were monitored at 30 °C using a microplate reader (Synergy HT from BioTek with Gene5 interface). The enzymatic activities have been measured as initial slopes of fluorescence intensity versus time.

Fluorescence Microscopy: Each sample (33.6×10^{-9} M DNA bp) was first mixed with YOYO-1 iodide (10×10^{-9} M) in 10×10^{-3} M Tris/HCl buffer (pH = 7.4). 10 µL drop was then deposited on a cover slip (Menzel–Gläser), and fluorescence microscopy observations were carried out with an AxioObserver D1 inverted microscope (Zeiss), equipped with a 100× oil immersion objective lens. Images were acquired with EMCCD camera (Photonmax 512B, Princeton Scientific) and Metavue image acquisition software (Molecular Devices).

Atomic Force Microscopy (AFM): AFM images were obtained in air at room temperature. A freshly cleaved mica surface (potassium aluminosilicate (Muscovite Mica) from Goodfellow) was first treated with 1×10^{-3} M spermine solution for 1 h, rinsed with an excess of MQ water. Right after removing water with filter paper (Whatman), a 20 µL drop of sample solution was placed on the mica slide. After 12 h of incubation in wet atmosphere, the mica plate was rinsed with an excess of MQ water and blown with compressed air. For the spermine-containing sample, bare mica was used for the IPDG adsorption. AFM measurements were performed using a 5100 Atomic Force Microscope (Agilent Technologies-Molecular Imaging) operated in a dynamic tip deflection mode (acoustic alternating current mode). All AFM experiments were performed using silicon probes (Applied NanoStructures-FORT) in the tapping mode with a spring constant of 3 N m^{-1} at 69 kHz. All AFM images are displayed with a height scale between –1.1 and +0.7 nm.

Supporting Information

Supporting Information is available from the Wiley Online Library or from the author.

Acknowledgements

This work was supported by the European Research Council (ERC) (European Community's Seventh Framework Programme (FP7/2007–2013)/ERC Grant Agreement No. 258782).

Conflict of Interest

The authors declare no conflict of interest.

 © 2017 Wiley-VCH Verlag GmbH & Co. KGaA, Weinheim

[1] N. C. Seeman, *Nature* **2003**, *421*, 427.
[2] N. C. Seeman, *Annu. Rev. Biochem.* **2010**, *79*, 65.
[3] P. W. K. Rothemund, *Nature* **2006**, *440*, 297.
[4] B. Saccà, C. M. Niemeyer, *Angew. Chem. Int. Ed.* **2012**, *51*, 58.
[5] F. Zhang, J. Nangreave, Y. Liu, H. Yan, *J. Am. Chem. Soc.* **2014**, *136*, 11198.
[6] S. Biffi, R. Cerbino, F. Bomboi, E. M. Paraboschi, R. Asselta, F. Sciortino, T. Bellini, *Proc. Natl. Acad. Sci. USA* **2013**, *110*, 15633.
[7] S. Biffi, R. Cerbino, G. Nava, F. Bomboi, F. Sciortino, T. Bellini, *Soft Matter* **2015**, *11*, 3132.
[8] C. Li, X. Zhou, Y. Shao, P. Chen, Y. Xing, Z. Yang, Z. Li, D. Liu, *Mater. Chem. Front.* **2017**, *1*, 654.
[9] J. Li, L. Mo, C. Lu, T. Fu, H. Yang, W. Tan, *Chem. Soc. Rev.* **2016**, *45*, 1410.
[10] X. Xiong, C. Wu, C. Zhou, G. Zhu, Z. Chen, W. Tan, *Macromol. Rapid Commun.* **2013**, *34*, 1271.
[11] Y. Shao, H. Jia, T. Cao, D. Liu, *Acc. Chem. Res.* **2017**, *50*, 659.
[12] J. B. Lee, Y. H. Roh, S. H. Um, H. Funabashi, W. Cheng, J. J. Cha, P. Kiatwuthinon, D. A. Muller, D. Luo, *Nat. Nanotechnol.* **2009**, *4*, 430.
[13] J. Li, C. Zheng, S. Cansiz, C. Wu, J. Xu, C. Cui, Y. Liu, W. Hou, Y. Wang, L. Zhang, I. Teng, H.-H. Yang, W. Tan, *J. Am. Chem. Soc.* **2015**, *137*, 1412.
[14] M. Nishikawa, Y. Mizuno, K. Mohri, N. Matsuoka, S. Rattanakiat, Y. Takahashi, H. Funabashi, D. Luo, Y. Takakura, *Biomaterials* **2011**, *32*, 488.
[15] J. Jin, Y. Xing, Y. Xi, X. Liu, T. Zhou, X. Ma, Z. Yang, S. Wang, D. Liu, *Adv. Mater.* **2013**, *25*, 4714.
[16] F. Topuz, S. Singh, K. Albrecht, M. Möller, J. Groll, *Angew. Chem. Int. Ed.* **2016**, *55*, 12210.
[17] C. Fernández-Solis, Y. Kuroda, A. Zinchenko, S. Murata, *Colloids Surf., B* **2015**, *129*, 146.
[18] T. Amiya, T. Tanaka, *Macromolecules* **1987**, *20*, 1162.
[19] Y. Xing, E. Cheng, Y. Yang, P. Chen, T. Zhang, Y. Sun, Z. Yang, D. Liu, *Adv. Mater.* **2011**, *23*, 1117.
[20] E. Cheng, Y. Xing, P. Chen, Y. Yang, Y. Sun, D. Zhou, L. Xu, Q. Fan, D. Liu, *Angew. Chem. Int. Ed.* **2009**, *48*, 7660.
[21] S. H. Um, J. B. Lee, N. Park, S. Y. Kwon, C. C. Umbach, D. Luo, *Nat. Mater.* **2006**, *5*, 797.
[22] J. B. Lee, S. Peng, D. Yang, Y. H. Roh, H. Funabashi, N. Park, E. J. Rice, L. Chen, R. Long, M. Wu, D. Luo, *Nat. Nanotechnol.* **2012**, *7*, 816.
[23] Y. Min, J. M. Caster, M. J. Eblan, A. Z. Wang, *Chem. Rev.* **2015**, *115*, 11147.
[24] Y. Sasaki, K. Akiyoshi, *Chem. Rec.* **2010**, *10*, 366.
[25] M. Molina, M. Asadian-Birjand, J. Balach, J. Bergueiro, E. Miceli, M. Calderón, *Chem. Soc. Rev.* **2015**, *44*, 6161.
[26] W. Sun, T. Jiang, Y. Lu, M. Reiff, R. Mo, Z. Gu, *J. Am. Chem. Soc.* **2014**, *136*, 14722.
[27] Y. H. Roh, J. B. Lee, S. J. Tan, B. Kim, H. Park, E. J. Rice, D. Luo, *Macromol. Rapid Commun.* **2010**, *31*, 1207.
[28] D. Costa, A. J. M. Valente, J. Queiroz, *J. Biotechnol.* **2015**, *202*, 98.
[29] D. Costa, A. J. M. Valente, J. Queiroz, *Colloids Surf., B* **2015**, *132*, 194.
[30] G. S. Chauhan, *Polym. Int.* **2014**, *63*, 1889.
[31] Y. Nomura, Y. Sasaki, M. Takagi, T. Narita, Y. Aoyama, K. Akiyoshi, *Biomacromolecules* **2005**, *6*, 447.
[32] T. Nochi, Y. Yuki, H. Takahashi, S. Sawada, M. Mejima, T. Kohda, N. Harada, I. G. Kong, A. Sato, N. Kataoka, D. Tokuhara, S. Kurokawa, Y. Takahashi, H. Tsukada, S. Kozaki, K. Akiyoshi, H. Kiyono, *Nat. Mater.* **2010**, *9*, 572.
[33] P. Song, K. Tapley, *Photochem. Photobiol.* **1979**, *29*, 1177.
[34] N. M. Green, *Biochem. J.* **1965**, *94*, 23C.
[35] S. Rudiuk, A. Venancio-Marques, G. Hallais, D. Baigl, *Soft Matter* **2013**, *9*, 9146.
[36] C. M. Niemeyer, M. Adler, B. Pignataro, S. Lenhert, S. Gao, L. Chi, H. Fuchs, D. Blohm, *Nucleic Acids Res.* **1999**, *27*, 4553.
[37] Y. Tian, Y. He, A. E. Ribbe, C. Mao, *Org. Biomol. Chem.* **2006**, *4*, 3404.
[38] A. Estévez-Torres, D. Baigl, *Soft Matter* **2011**, *7*, 6746.
[39] L. Cinque, Y. Ghomchi, Y. Chen, A. Bensimon, D. Baigl, *ChemBioChem* **2010**, *11*, 340.
[40] S. Rudiuk, A. Venancio-Marques, D. Baigl, *Angew. Chem. Int. Ed.* **2012**, *51*, 12694.
[41] A. Venancio-Marques, A. Bergen, C. Rossi-Gendron, S. Rudiuk, D. Baigl, *ACS Nano* **2014**, *8*, 3654.
[42] M. Y. Ono, E. M. Spain, *J. Am. Chem. Soc.* **1999**, *121*, 7330.
[43] Y. Wang, S. Ran, B. Man, G. Yang, *Soft Matter* **2011**, *7*, 4425.
[44] A. Küchler, M. Yoshimoto, S. Luginbühl, F. Mavelli, P. Walde, *Nat. Nanotechnol.* **2016**, *11*, 409.
[45] M. Glettenberg, C. M. Niemeyer, *Bioconjugate Chem.* **2009**, *20*, 969.
[46] Z. Zhao, J. Fu, S. Dhakal, A. Johnson-Buck, M. Liu, T. Zhang, N. W. Woodbury, Y. Liu, N. G. Walter, H. Yan, *Nat. Commun.* **2016**, *7*, 10619.
[47] Y. Fu, D. Zeng, J. Chao, Y. Jin, Z. Zhang, H. Liu, D. Li, H. Ma, Q. Huang, K. V. Gothelf, C. Fan, *J. Am. Chem. Soc.* **2013**, *135*, 696.
[48] Y. Zhang, S. Tsitkov, H. Hess, *Nat. Commun.* **2016**, *7*, 13982.
[49] A. Estévez-Torres, C. Crozatier, A. Diguet, T. Hara, H. Saito, K. Yoshikawa, D. Baigl, *Proc. Natl. Acad. Sci. USA* **2009**, *106*, 12219.
[50] A. Diguet, N. K. Mani, M. Geoffroy, M. Sollogoub, D. Baigl, *Chem. Eur. J.* **2010**, *16*, 11890.
[51] S. Rudiuk, K. Yoshikawa, D. Baigl, *Soft Matter* **2011**, *7*, 5854.

Received: March 2, 2017
Revised: April 11, 2017
Published online: May 31, 2017

 © 2017 Wiley-VCH Verlag GmbH & Co. KGaA, Weinheim